An instant change of elastic lattice strain during Cu_2Se phase transition: origin of abnormal thermoelectric properties

Hui Bai[1,2†], Xianli Su[1†], Dongwang Yang[1], Qingjie Zhang[1], Gangjian Tan[1], Ctirad Uher[3], Xinfeng Tang[1*] and Jinsong Wu[1,2*]

[1]*State Key Laboratory of Advanced Technology for Materials Synthesis and Processing, Wuhan University of Technology, Wuhan 430070, China*

[2]*Nanostructure Research Center, Wuhan University of Technology, Wuhan 430070, China*

[3]*Department of Physics, University of Michigan, Ann Arbor, Michigan 48109, USA*

[†]These authors contributed equally to this work.

* Correspondence and requests for materials should be addressed to Jinsong Wu (wujs@whut.edu.cn) and Xinfeng Tang (tangxf@whut.edu.cn).

This is the author manuscript accepted for publication and has undergone full peer review but has not been through the copyediting, typesetting, pagination and proofreading process, which may lead to differences between this version and the Version of Record. Please cite this article as doi: 10.1002/adma.202100431.

Abstract: The superionic conductor Cu_2Se is a promising thermoelectric material due to its low thermal conductivity. An abnormal but clear change in the thermoelectric parameters has been observed during the phase transformation from the ordered and non-cubic α-Cu_2Se to the disordered and cubic β-Cu_2Se. However, the microstructural origin of the abnormal change and its implications for thermoelectric applications remain largely unknown. Herein, by mimicking the real working conditions of thermoelectrics, the phase transition from α- to β-Cu_2Se induced by the rising temperature has been carefully investigated by *in-situ* transmission electron microscopy. It is observed that an abrupt and anisotropic volume-change in the Se-sublattice occurs when the temperature is raised to the phase transition point. The abnormal change in the crystalline volume *versus* temperature, which is caused by the local migration of Cu-ions, induces an instant and uncommon strain-field, which reduces the carrier's mobility and increases the electrical resistance. Local migration of Cu-ions is responsible for a quite low thermal conductivity. Such effects exit only at the instant of the phase transition. Observing the thermoelectric response of the structure during the phase transition may provide insights into the development of high performance thermoelectric materials, which fall beyond the traditional approaches.

1. Introduction

Thermoelectric technology is a promising approach of generating clean energy from waste heat, including the heat from automobile's exhaust systems, solar energy, and geothermal energy[1]. Advances in the thermoelectric technology rely on the discovery of highly efficient thermoelectric materials. The efficiency of a thermoelectric (TE) material is gauged by its dimensionless thermoelectric figure of merit ZT, defined as $ZT = \alpha^2\sigma T/(\kappa_L+\kappa_e)$, where α, σ, κ_L, κ_e, and T are the Seebeck coefficient, electrical conductivity, lattice thermal conductivity, electronic thermal conductivity, and the absolute temperature, respectively[2].

Cu_2Se is one of the so-called 'liquid-like' thermoelectric materials, often referred to as "phonon-liquid electron-crystal" structure[3]. In the crystal lattice, Se-anions constitute a rigid cubic sub-lattice while Cu cations form a liquid-like sub-lattice, and thus have a rather high mobility[3a, 4]. Due to its 'liquid-like' structure, Cu_2Se has an intrinsically ultralow lattice thermal conductivity, an important aspect for an efficient thermoelectric[5]. Moreover, Cu_2Se (and other liquid-like materials) show an exceptionally good electronic transport property, which are believed to be associated with the rigid Se sub-lattice. Therefore, high ZT values above 2 were attained in Cu_2Se, which shows great perspective

for commercial applications in power generation recycling the waste heat at high temperature[6]. However, noted that this 'half-solid half-liquid' nature of the structure gives rise to the 'abnormal' transport properties. A striking feature of Cu_2Se is its abnormal transport behavior observed in the temperature range between 340 K and 400 K, where a phase transition from the ordered α-Cu_2Se phase to the disordered β-Cu_2Se phase takes place[7]. Within the narrow range of the α to β phase transition, the so-called critical scattering regime for phonons and electrons, ingenious experimental designs were developed to make transport measurements under precisely controlled temperature[8]. Under an unusual transport measurements, an extremely high Seebeck coefficient and *ZT* (as high as 400) have been reported [9]. Under the usual conditions of transport measurements, it was also shown that the *ZT* has increased by a factor of about ~3-7 times at the phase transition temperature [4c, 8]. However, the underlying mechanism of the abnormal behavior remains largely unclear and thus its potential impact on the development of high performance thermoelectric materials, by utilizing the above extraordinary properties, has not yet materialized.

In this paper, the dynamical microstructural evolution of Cu_2Se during the α to β phase transition has been carefully studied to reveal the microstructural mechanism of the critical scattering and the origin of the abnormal thermoelectric properties. When a thermoelectric

material operates as a power generator or as an electronic cooler, it is exposed to a temperature gradient. With the development of *in-situ* transmission electron microscopy (TEM)[10], microstructural evolutions can be monitored by both imaging and diffraction while the temperature is varied. Adopting the latest technical advances, we have observed an abrupt change in the lattice strain in Cu_2Se during the phase transition. We believe this provides a novel insight into the cause of the observed critical scattering.

2. Results and Discussion

Microstructural changes and crystalline evolution in the Cu_2Se sample prepared by the method of self-propagating high-temperature synthesis (SHS) were studied by *in-situ* TEM. The temperature was gradually increased to induce the α-Cu_2Se to β-Cu_2Se phase transition (please refer to a supplementary Video S1). While the high temperature β-Cu_2Se has a face-centered cubic structure (a = 5.84 Å), at room temperature Cu_2Se is in its monoclinic α-Cu_2Se phase[7b] (a = 7.148 Å, b = 12.349 Å, c = 13.833 Å, β=100°, space group of C2/*C*). According to the previous studies of the α-Cu_2Se structure[7a-d], although there are many α-Cu_2Se variants, we found that all observed electron diffraction patterns could be indexed using this structure. As shown in Figure 1(a) and Figure S1 (with spots

being indexed), two α-Cu_2Se crystals separated by a grain boundary can be identified, one oriented along the [0-10] direction and the other along the [10-1] direction. When heated up to 383 K, the two crystals remained in the α-Cu_2Se phase, while based on the observed image contrast, the density of dislocations and stacking faults created due to the fast non-equilibrium self-propagating high-temperature synthesis (SHS) process was greatly reduced in the two crystals (Figure 1b). At the temperature of 388 K, based on the disappearance of the superlattice spots (as marked by white arrowheads in Figure 1c), a phase transition from α-Cu_2Se [10-1] to β-Cu_2Se [110] has commenced. However, the α-Cu_2Se [0-10]-oriented crystal has not transformed into the β-Cu_2Se [110] phase until the temperature reached 393 K. This is shown in Figure 1d, where the superlattice spots identifying the α-Cu_2Se [0-10] crystal have disappeared. The atomic structure of the two α-Cu_2Se crystals and of β-Cu_2Se are shown in Figures 1e-g, respectively. Their experimental selected area electron diffraction (SAED) patterns are compared to the simulated patterns to confirm the correctness of the crystalline indexes in Figure S2.

It is a surprising observation that the critical phase transition temperature depends on the orientation of the α-Cu_2Se domains. In our *in-situ* TEM experiment, we kept the temperature at 388 K for more than an hour (~68 min) and the α-Cu_2Se [0-10]- oriented crystal remained stable (Figure S3). At the moment the temperature was increased to 393

K, we observed instantly the formation of β-Cu_2Se. This suggests that the phase transformation is not related to the Cu-ions' gradual (or thermal) diffusion, but is closely correlated to a sudden Cu-ion's hopping among sites with quantized energy levels.

Along with the hopping of Cu-ions from ordered sites to disordered ones, there is also an elastic contraction and/or expansion of the Se-sublattice due to the phase transformation, which induces a large elastic strain in the system with mixed α and β-Cu_2Se phases. The Se-sublattice has a *fcc* structure and can be identified by the strong diffraction spots as marked by purple arrowheads in Figure 1(a-d). An overlap of the diffraction patterns of the α-Cu_2Se [10-1] domain, α-Cu_2Se [0-10] domain and β-Cu_2Se [110] is shown in Figure S4, in which the mismatch among the domains can be clearly seen. As shown in Figure S4b, when the lattice parameter of β-Cu_2Se is used as the reference, the pseudo-cubic parameter *a* of the α-Cu_2Se [10-1] domain and [0-10] domain is different. This is especially so in the phase transformation from the α-Cu_2Se [0-10] domain to β-Cu_2Se [110], where the *d*-spacing of the (-202) plane becomes large, while that of the (004) plane is reduced. This induces an anisotropic elastic strain in the Se-sublattice.

The resemblance of the α-Cu_2Se [10-1] domain to the β-Cu_2Se [110] structure leads to a lower transition temperature (compared to that between the α-Cu_2Se [0-10] domain and

β-Cu_2Se [110]), implying that the strain mismatch in the domains does change the critical energy needed for the phase transformation. In other words, under a small mismatch, hopping of Cu-ions and contraction/expansion of the Se-sublattice are more energetically favorable and the phase transformation is easier to occur. Indeed, the atomic structure of the α-Cu_2Se [10-1] crystal looks very similar to that of β-Cu_2Se [110], as shown in Figure 2. Although the HAADF STEM image collected from the α-Cu_2Se [10-1] crystal (Figure 2a) is very alike to that of the β-Cu_2Se [10-1] crystal (Figure 2b), the two phases can be distinguished by their Fast Fourier Transform (FFT) patterns. While the superlattice spots can be found in the FFT pattern of the α-phase (insert in Figure 2a), they are not present in the β phase. There is a closed crystalline orientation relationship between the two phases during the phase transformation: *e.g.* α_[10-1] // β_[110], α_(202) // β_(002), and α_(060) // β_(2-20), as illustrated in Figure 2c. The subtle difference in the Cu-ions clusters between the two phases can also be seen by carefully examining the STEM images (Figs. d and e), where a symmetric distribution of Cu-ions around Se was found in β-Cu_2Se. This could be the reason why the α-Cu_2Se [10-1]-oriented crystal showed a slightly lower thermal stability than the α-Cu_2Se [0-10] crystal. From the morphological changes along with the temperature rise (Figure S5), it could be surmised that the defect density has gradually decreased at higher and higher temperatures. When both α-Cu_2Se crystals

transformed into β-Cu_2Se at 393K, the major defects present were dislocations located at the boundary of the two α-Cu_2Se crystals (Figure S6).

The phase transformation between β-Cu_2Se and various α-Cu_2Se domains is in general reversible. While there is only one high temperature cubic β-Cu_2Se structure, there are many α-Cu_2Se domains forming at low-temperatures. We then explored whether the phase transformation was reversible and found that, in general, the original α-Cu_2Se domain structure was recovered upon lowering the temperature. However, there were also exceptions. As shown in Figure 3 and supplementary videos S2-5, the phase transformation between the α-Cu_2Se [1-21] domain (the original domain) and the β-Cu_2Se crystal along the [112] direction was observed repeatedly by TEM *via in-situ* heating. Every time the temperature was higher than the phase transformation temperature, the [112] β-Cu_2Se crystal forms. When the temperature was kept below the phase transformation temperature (*e.g.*, at 373K), the α-Cu_2Se [1-21] domain was observed 11 times out of 13 cycles. In the other 2 cycles, the α-Cu_2Se [100] domain formed (as shown in Figure 3c). During the phase transformation, one set of the parallel lattice planes among the three domains is β-Cu_2Se (11-1) // α-$Cu_2Se_{[1\text{-}21]}$(-202) // α-$Cu_2Se_{[100]}$(004). The d-spacing of the lattice planes are $d_{\beta\text{-}Cu2Se(11\text{-}1)}$ = 3.389 Å, $d_{\alpha\text{-}Cu2Se(\text{-}202)}$ = 3.375 Å (with 0.4% mismatch to that of β phase) and $d_{\alpha\text{-}Cu2Se(004)}$ = 3.406 Å (with 0.5% mismatch to that of β phase), respectively.

In another crystal orientation the d-spacing of the lattice planes are d_{β}-Cu_2Se(2-20) = 2.076 Å, d_{α}-Cu_2Se(060) = 2.058 Å (with 0.9% mismatch to that of β phase) and d_{α}-Cu2Se(135) = 2.076 Å (no mismatch), respectively. Here, the phase transformation proceed preferentially through a route with the least mismatch (and thus minimal mismatch strain).

An instant buildup and release of the elastic strain at the moment the phase transformation takes place has been observed by *in-situ* high resolution STEM. The buildup of the elastic strain is mainly due to large volumetric changes (between α and β phases), while the release of the strain is through lattice vibrations. One example is the vibration with the frequency of ~10 Hz. As shown in Figure 4 and Video S6, the STEM images of both the α-phase at a room temperature (Figure 4a) and β-phase at 423 K (Figure 4b) clearly show that the sample under observation is quite stable with no vibrational motion. However, the STEM image (Figure 4h) recorded at 390 K (when the phase transformation was taking place) depicts the obvious nearly-periodic interference fringes. Such fringes are generated by specimen vibrations (since the other possible interfering factors, such as magnetic/electric field *etc*., can be excluded). The frequency of vibrations was calculated by analyzing the FFT of the image as 10 Hz, meaning there are about 10 vibrations in a second observed in the experiment.

The variation of several key thermoelectric parameters of the prepared Cu_2Se samples with the rising temperature was measured across the α-Cu_2Se to β-Cu_2Se phase transformation, as shown in Figure S7. The major abnormal changes during the phase transformation are: 1) the resistivity has suddenly increased, 2) the thermal conductivity dramatically decreased[8], 3) the carrier concentration and the mobility precipitously decreased.

According to our investigations, the microstructural origin of the abnormal thermoelectric behavior can be better understood in terms of a suddenly developed strain during the α- to β-Cu_2Se phase transformation. The electrical conductivity is mainly influenced by the Se-sublattice, which is the backbone for the charge carrier transport. Elastic deformations of the Se-sublattice during the phase transformation make it difficult for the charge carriers to go through smoothly and the electrical resistivity thus tends to increase. The dominant charge carrier in α-Cu_2Se is the electron-hole pairs formed in the crystal, which are influenced by the elastic strain (as the strain is correlated with the distribution of Cu-ion vacancies). Thus, along with the order-to-disorder transition in the Cu-ions occupancy during the phase transformation, the electronic structure has also changed suddenly[11]. As such, the phase transformation causes sudden changes in most of the thermoelectric parameters:

1) The appearance of localized strain fields reduces the carrier mobility and thus increases the resistivity, which could be one of the origins of the critical scattering of electrons [4c, 8b].

2) The strain induced by the phase transformation (lattice contraction or expansion happens when α-Cu_2Se is transformed into β-Cu_2Se), modifies not only the electronic structure, but also the carries concentration, which is consistent with previous observations[4c, 11].

3) The collective and sudden migration of Cu-ions (from the ordered sites to the disordered sites), enhances scattering of phonons, leading to a large decease in the thermal conductivity.

From the experimental results (where different α-domains have different transformation temperatures), it is obvious that elastic strains play an important role in modulating the thermodynamic properties during the Cu_2Se phase transformation. Consequently, there are large and rapid changes in the elastic strain within the Se-sublattice during the phase transformation. While the elastic strain will not destroy the integrity of the Se-lattice, it greatly reduces the electrical conductivity as the strain has a huge impact on the electronic structure. However, the effects will quickly disappear as soon as the strain is released. Thus, the abnormal thermoelectric behavior appears usually only within a very short time period. Proper design of materials with appropriate attentions to a stable strain

distribution (strain engineering) might be an effective way in the development of novel high-performing thermoelectrics.

3. Conclusion

By applying *in-situ* TEM, a dynamic evolution of the crystalline structure as well as the strain fields accompanying the elastic deformation of the Se-sublattice during the α-Cu_2Se to β-Cu_2Se phase transformation have been carefully studied. α-Cu_2Se domains with different orientations show different critical transformation temperatures, which implies that strain plays an important role in the transformation process. The smaller the mismatch between the α-Cu_2Se domain and the β-Cu_2Se domain, the lower the transformation temperature. The generation and release of a large elastic strain at an instant the phase transformation takes place has been observed and found as one of the main origins of the abnormal thermoelectric behavior of Cu_2Se.

4. Experimental Section

Polycrystalline Cu_2Se samples were prepared by the method of SHS[5a]. High purity powers of Cu (99.95%) and Se (99.99%) were weighed out according to the stoichiometric ratio of 2:1 and mixed homogeneously in an agate mortar. A pellet with a diameter of 10 mm was prepared from the mixed powders by uniaxial cold pressing under

10 MPa for 5 min. The pellets were ignited in vacuum to obtain polycrystalline ingots containing solely the Cu_2Se α-phase. The ingots were then ground into powder using again the agate mortar to attain a homogeneous powder of Cu_2Se. The obtained powder was sintered by plasma activated sintering (PAS) (PAS-III-Ed, Elenix, Japan) using a carbon mold under 40 MPa in vacuum at 973 K for 3 min.

The as-prepared ingot was sectioned by focused ion beam (FIB) milling (Helios Nanolab G3 UC, FEI) for the structural characterization. *Ex-situ* and *in-situ* TEM characterizations of the samples were carried out by transmission electron microscopy (Talos F200s, FEI) and double C_S-corrected transmission electron microscopy (Titan Themis G2 60-300, FEI). *In-situ* experiments using a nano-chip electrical and thermal holder (Dens solutions) were performed. For all of the *in-situ* heating TEM experiments, the heating rate is 1°C/s and the samples been heated are hold for 1 minutes before the TEM images and diffraction patterns are collected (to ensure a stable temperature has reached).

The high temperature resistance and the Hall coefficient (R_H) from RT to 475 K were measured using the van der Pauw technique under a reversible magnetic field of 1.5 T. The effective carrier concentration (n_H) was calculated from $n_H = 1/eR_H$, where e is the electron charge. The Hall mobility followed from $\mu_H = \sigma R_H$.

Supporting Information

Figures S1-S7

Videos S1-S6

Acknowledgements

The work is supported by the National Natural Science Foundation of China (52072282). The authors wish to acknowledge support from the National Key Research and Development Program of China (Grant No. 2019YFA0704900). The S/TEM work was performed at the Nanostructure Research Center (NRC), which is supported by the Fundamental Research Funds for the Central Universities (WUT: 2020III002GX), State Key Laboratory of Advanced Technology for Materials Synthesis and Processing. the

Conflict of Interest

The authors declare no conflict of interest.

Keywords

thermoelectric material, phase transformation, *in-situ* TEM, elastic lattice strain, Cu_2Se ionic conductor.

References and notes:

[1] H. J. Goldsmid, *Introduction to thermoelectricity*, Springer, **2010**.

[2] a) D. M. Rowe, *Thermoelectrics handbook: macro to nano*, CRC press, **2018**; b) G. Tan, L. D. Zhao, M. G. Kanatzidis, *Chem. Rev.* **2016**, 116, 12123; c) X. L. Shi, J. Zou, Z. G. Chen, *Chem. Rev.* **2020**, 120, 7399.

[3] a) H. Liu, X. Shi, F. Xu, L. Zhang, W. Zhang, L. Chen, Q. Li, C. Uher, T. Day, G. J. Snyder, *Nat. Mater.* **2012**, 11, 422; b) K. Zhao, P. Qiu, X. Shi, L. Chen, *Adv. Funct. Mater.* **2019**, 30.

[4] a) K. Trachenko, *Phys. Rev. B* **2008**, 78; b) P. Lu, H. Liu, X. Yuan, F. Xu, X. Shi, K. Zhao, W. Qiu, W. Zhang, L. Chen, *J. Mater. Chem. A* **2015**, 3, 6901; c) H. Liu, X. Yuan, P. Lu, X. Shi, F. Xu, Y. He, Y. Tang, S. Bai, W. Zhang, L. Chen, Y. Lin, L. Shi, H. Lin, X. Gao, X. Zhang, H. Chi, C. Uher, *Adv. Mater.* **2013**, 25, 6607.

[5] a) X. Su, F. Fu, Y. Yan, G. Zheng, T. Liang, Q. Zhang, X. Cheng, D. Yang, H. Chi, X. Tang, *Nat. Commun.* **2014**, 5, 1; b) R. Nunna, P. Qiu, M. Yin, H. Chen, R. Hanus, Q. Song, T. Zhang, M.-Y. Chou, M. T. Agne, J. He, G. J. Snyder, X. Shi, L. Chen, *Energy Environ. Sci.* **2017**, 10, 1928; c) J.-Y. Tak, W. H. Nam, C. Lee, S. Kim, Y. S. Lim, K. Ko, S. Lee, W.-S. Seo, H. K. Cho, J.-H. Shim, C.-H. Park, *Chem. Mater.* **2018**, 30, 3276; d) S. Namsani, S. Auluck, J. K. Singh, *Appl. Phys. Lett.* **2017**, 111; e) H. Tang, F.-H. Sun, J.-F. Dong, Asfandiyar, H.-L. Zhuang, Y. Pan, J.-F. Li, *Nano Energy* **2018**, 49, 267; f) M. Li, D. L. Cortie, J. Liu, D. Yu, S. M. K. N. Islam, L. Zhao, D. R. G. Mitchell, R. A. Mole, M. B. Cortie, S. Dou, X. Wang, *Nano Energy* **2018**, 53, 993; g) A. A. Olvera, N. A. Moroz, P. Sahoo, P. Ren, T. P. Bailey, A. A. Page, C. Uher, P. F. P. Poudeu, *Energy Environ. Sci.* **2017**, 10, 1668; h) J. L. Niedziela, D. Bansal, A. F. May, J. Ding, T. Lanigan-Atkins, G. Ehlers, D. L. Abernathy, A. Said, O. Delaire, *Nat. Phys.* **2019**, 15, 73; i) D. Voneshen, H. Walker, K. Refson, J. Goff, *Phys. Rev. Lett.* **2017**, 118, 145901.

[6] a) Y. He, T. Day, T. Zhang, H. Liu, X. Shi, L. Chen, G. J. Snyder, *Adv. Mater.* **2014**, 26, 3974; b) W. D. Liu, L. Yang, Z. G. Chen, J. Zou, *Adv. Mater.* **2020**, 32, 1905703.

[7] a) A. Skomorokhov, D. Trots, M. Knapp, N. Bickulova, H. J. J. o. a. Fuess, *J. Alloys Compd.* **2006**, 421, 64; b) W. Qiu, P. Lu, X. Yuan, F. Xu, L. Wu, X. Ke, H. Liu, J. Yang, X. Shi, L. Chen, J. Yang, W. Zhang, *J. Chem. Phys.* **2016**, 144, 194502; c) L. Gulay, M. Daszkiewicz, O. Strok, A. Pietraszko, *Chem. Met. Alloy* **2011**, 200; d) H. Chi, H. Kim, J. C. Thomas, G. Shi, K. Sun, M. Abeykoon, E. S. Bozin, X. Shi, Q. Li, X. Shi, *Phys. Rev. B* **2014**, 89, 195209; e) S. A. Danilkin, M. Avdeev, M. Sale, T. Sakuma, *Solid State Ionics* **2012**, 225, 190; f) E. Eikeland, A. B. Blichfeld, K. A. Borup, K. Zhao, J. Overgaard, X. Shi, L. Chen, B. B. Iversen, *IUCrJ* **2017**, 4, 476; g) T. Zhao, Y.-A. Wang, Z.-Y. Zhao, Q. Liu, Q.-J. Liu, *Mater. Res. Express* **2018**, 5; h) P. Lu, W. Qiu, Y. Wei, C. Zhu, X. Shi, L. Chen, F. Xu, *"Acta Crystallogr., Sect. B: Struct. Sci."* **2020**, 76, 201.

[8] a) H. Liu, X. Shi, M. Kirkham, H. Wang, Q. Li, C. Uher, W. Zhang, L. Chen, *Mater. Lett.* **2013**, 93, 121; b) H. Chen, Z. Yue, D. Ren, H. Zeng, T. Wei, K. Zhao, R. Yang, P. Qiu, L. Chen, X. Shi, *Adv. Mater.* **2019**, 31, 1806518.

[9] D. Byeon, R. Sobota, K. Delime-Codrin, S. Choi, K. Hirata, M. Adachi, M. Kiyama, T. Matsuura, Y. Yamamoto, M. Matsunami, T. Takeuchi, *Nat. Commun.* **2019**, 10, 72.

[10] a) M. L. Taheri, E. A. Stach, I. Arslan, P. A. Crozier, B. C. Kabius, T. LaGrange, A. M. Minor, S. Takeda, M. Tanase, J. B. Wagner, *Ultramicroscopy* **2016**, 170, 86; b) T. W.

Hansen, J. B. Wagner, P. L. Hansen, S. Dahl, H. Topsøe, C. J. Jacobsen, *science* **2001**, 294, 1508.

[11] S. Sun, Y. Li, Y. Chen, X. Xu, L. Kang, J. Zhou, W. Xia, S. Liu, M. Wang, J. Jiang, A. Liang, D. Pei, K. Zhao, P. Qiu, X. Shi, L. Chen, Y. Guo, Z. Wang, Y. Zhang, Z. Liu, L. Yang, Y. Chen, *Science Bulletin* **2020**, 65, 1888.

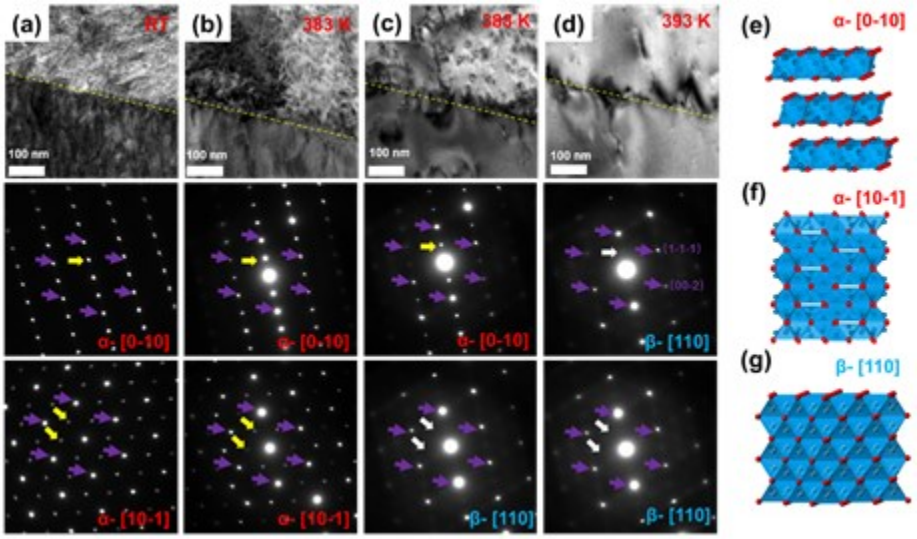

Figure 1. Change in the diffraction patterns and TEM images during heating of Cu_2Se. (a-d) TEM images and selected area electron diffraction on both sides of the grain boundary (yellow dotted line) at RT, 383 K, 388 K, and 393 K, respectively. The second row is the selected area electron diffraction of area 1, and the third row is the selected area electron diffraction of area 2. (e-g) Simulated structure of the α-Cu_2Se phase along the [0-10], [10-1] and of the β-Cu_2Se phase along the [110] directions, respectively.

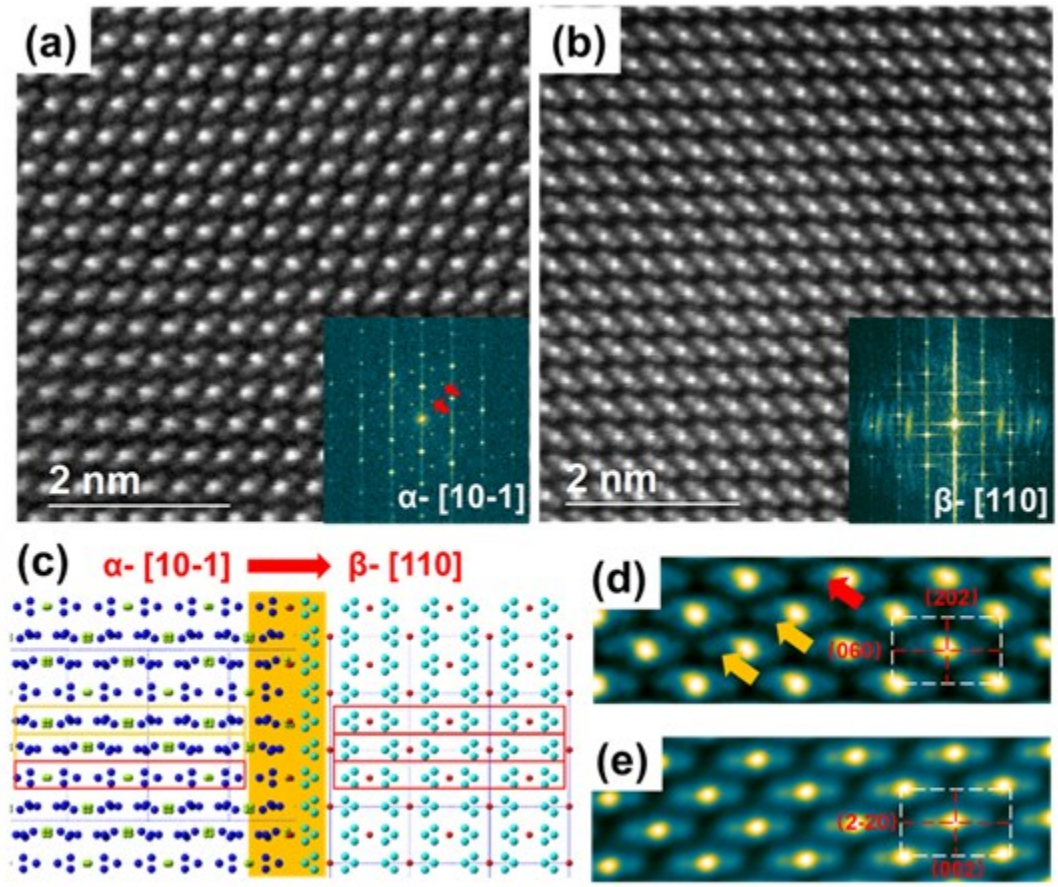

Figure 2. Structural contrast between the α-phase of Cu_2Se along the [10-1] direction and the β-phase along the [110] direction. (a,b) Atomic resolution HAADF-STEM images in the α-[10-1] and β-[110] directions. The insets are the corresponding FFT images. The red arrow points out the difference between the two phases. (c) Schematic diagram of atomic structure of the two phases. (d) Atomic images of the α-Cu_2Se along [10-1] directions at high magnifications. (e) Atomic images of the β-Cu_2Se along [110] directions at high magnifications.

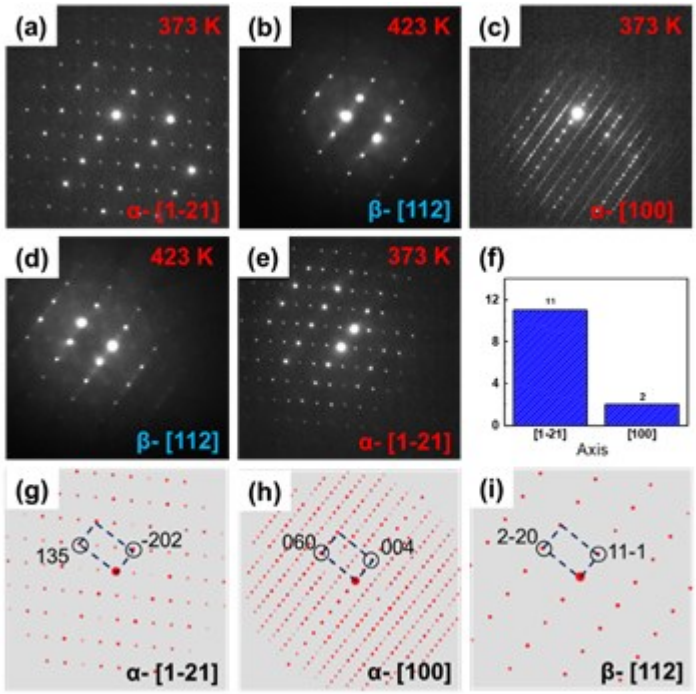

Figure 3. Phase changes during heating and cooling of Cu_2Se. (a-e) Selected area electron diffraction of the sample at 373 K, 423 K, 373 k, 423K, and 373 K during the heating and cooling process, respectively. (f) Distribution histogram of the sample's low temperature phase after cooling. (g-i) Simulated electron diffraction patterns of the α-phase of Cu_2Se along [1-21], [100] and of the β-phase of Cu_2Se along [112] directions, respectively.

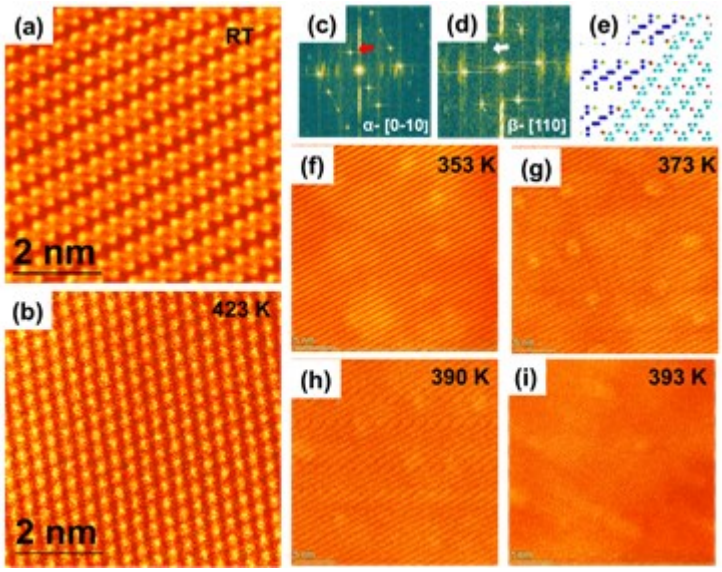

Figure 4. Changes in STEM images upon heating of Cu_2Se. (a-b) STEM images of Cu_2Se at RT and 423 K, respectively. (c-d) FFT image of (a) and (b), respectively. (e) Schematic diagram of the α-phase of Cu_2Se along [0-10] and the β-phase of Cu_2Se along [110] directions. (f-g) STEM images of Cu_2Se at 353 K, 373 K, 390 K and 393 K, respectively.

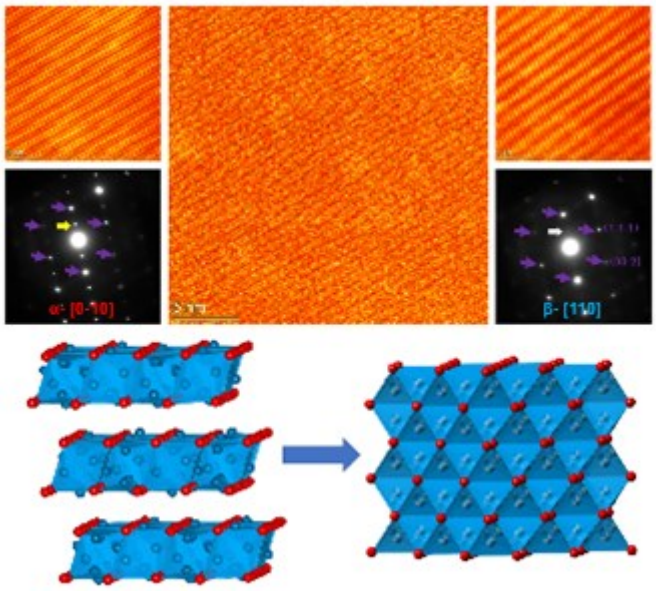

By applying *in-situ* TEM, a dynamic evolution of the crystalline structure and the strain fields during Cu_2Se phase transformation have been studied. The instant generation and release of a large elastic strain is identified as one of the main origins of the abnormal thermoelectric behavior of Cu_2Se in the moment of phase transition.